Indentation size effect in spherical and pyramidal indentations

IOP PUBLISHING JOURNAL OF PHYSICS D: APPLIED PHYSICS

J. Phys. D: Appl. Phys. **41** (2008) 074005 (5pp) doi:10.1088/0022-3727/41/7/074005

Indentation size effect in spherical and pyramidal indentations

Karsten Durst[1], **Mathias Göken**[1] **and George M Pharr**[2,3]

[1] University Erlangen–Nürnberg, Department of Materials Science and Engineering, 91058 Erlangen, Germany
[2] The University of Tennessee, Department of Materials Science and Engineering, Knoxville, TN 37996-2200, USA
[3] Oak Ridge National Laboratory, Materials Science and Technology Division, Oak Ridge, TN 37831, USA

E-mail: karsten.durst@ww.uni-erlangen.de, m.goeken@ww.uni-erlangen.de and pharr@utk.edu

Received 6 August 2007, in final form 15 January 2008
Published 12 March 2008
Online at stacks.iop.org/JPhysD/41/074005

Abstract

The indentation size effect (ISE) is studied for spherical and pyramidal indentations on a Ni poly-crystal. The indentation experiments were conducted using a Berkovich geometry as well as different spherical indenters with radii of 0.38, 3.8 and 51.0 μm. A strong ISE is observed for the material yielding a higher hardness at smaller depths or smaller sphere radii. The transition from elastic to plastic behaviour is associated with a pop-in in the load–displacement curve, in contrast to the conventional elastic–plastic transition as discussed by Tabor. The indentation response is modelled using Tabor's approach in conjunction with the uniaxial macroscopic stress–strain behaviour for calculating the statistically stored dislocation density for a given indenter geometry. The geometrically necessary dislocation (GND) density is calculated using a modified Nix/Gao approach, whereas the storage volume for GNDs is used as a parameter for the measured depth dependence of hardness. It will be shown that the ISE for both pyramidal and spherical indentations is related and can be understood within the same given framework. The indentation response of metallic materials can thus be modelled from pop-in to macroscopic hardness.

(Some figures in this article are in colour only in the electronic version)

1. Introduction

Increasing strength at small length scale has been observed in many metallic systems. Microbending and microtorsion experiments have led to the development of a model of strain gradient plasticity, which describes the observed increasing strength of the material, using a phenomenological inner material length scale [1]. In indentation testing, similar size effects can be observed at different indentation depths. Crystalline materials often show a discrete transition from elastic to plastic deformation at an indentation depth <100 nm, which is referred to as the pop-in behaviour. Below the pop-in event, the materials show an extraordinarily high strength, which is close to the theoretical strength of the crystal itself [2, 3]. After the pop-in, the material deforms elastic–plastically. The initially very high plastic hardness decreases, until at higher indentation depths a depth-independent hardness is found. This is referred to as the indentation size effect (ISE) [4].

The ISE has been successfully modelled by Nix and Gao (NG) [5], using the Taylor dislocation model. The ISE is there directly related to geometrically necessary dislocations [6] (GNDs), whose density is proportional to the inverse of the indentation depth. Recently a correction to the NG model of the ISE was proposed, considering the size of the plastic zone [7, 8]. The ISE has been studied intensively for pyramidal and spherical indentation [9–16, 21]. Electron backscatter diffraction experiments revealed strong local orientation gradient around nanoindents [14, 15]. Lim *et al* have shown that there is a size effect for spherical indentation, depending on the tip radius. For spherical indentations with a small tip radius, the material exhibits a higher deformation resistance [9]. Swadener *et al* have, moreover, related spherical indentation to conical indentation using the contact radius for relating size effects observed with the different indenter geometries [16].

In this paper the ISE for spherical indentation is modelled in the same framework as for conical indentation. Using

the approach of Atkins and Tabor [17] in conjunction with Taylor dislocation hardening and the Ashby concept on GNDs as discussed by Nix and Gao. The ISE is modelled for spherical and conical indentation. The model is supplemented by indentation testing on a Ni poly-crystal using three different spheres. The spherical indentation tests were complemented by Berkovich indentation.

2. Modelling approach

The following modelling approach is based on Tabor's concept of representative strain and on Ashby's approach for statistical and geometrically necessary dislocation hardening, as has been applied by Nix and Gao for discussing strain gradient plasticity. A detailed discussion of the modelling concept presented here can be found in [7]. There are several models for describing the hardening contribution of GNDs on the deformation resistance of materials, yielding some controversy in the literature about which model is physically correct or not [18]. In the approach used here, the total dislocation density ρ_{total} of both statistically stored dislocations (SSDs) and GNDs is used for calculating the average spacing l of dislocations ($(1/l) = \sqrt{\rho_{\text{SSD}} + \rho_{\text{GND}}} = \sqrt{\rho_{\text{total}}}$) as considered in the Taylor approach. This seems to be a reasonable way of describing the complicated dislocation microstructure underneath nanoindentations.

The modelling description starts with the macroscopic material behaviour. The SSD density is calculated using the representative strain ε_{rep} of a spherical indenter with a tip radius R in conjunction with the macroscopic work hardening behaviour of the material. The macroscopic flow stress σ_{pl} of a material is given as

$$\sigma_{\text{pl}} = \sigma_0 \varepsilon_{\text{pl}}^n, \tag{1}$$

$$\varepsilon_{\text{rep}} = 0.2\frac{a_{\text{c}}}{R}, \tag{2}$$

where ε_{pl} is the plastic strain, n the work hardening coefficient, a_{c} the contact radius, ε_{rep} the representative strain and σ_0 the strength coefficient. For a conical indenter, the representative strain is given by $0.2\tan\beta$, where β is the angle between the surface and the indenter.

The Taylor and Tabor approach relates the macroscopic hardness H_0 to the statistical stored dislocation density ρ_{SSD}, where C is a constraint factor, M the Taylor factor, α a statistical factor, ranging from 0.3 to 1.3. G is the shear modulus and b the magnitude of the Burgers vector and τ is the shear stress:

$$H_0 = C\sigma = MC\tau = MC\alpha Gb\sqrt{\rho_{\text{SSD}}(\varepsilon_{\text{rep}})}. \tag{3}$$

The same approach also applies to pyramidal indentation except that in pyramidal indentation the representative strain yields a discrete average strain for a given opening angle of the indenter.

The GND density ρ_{GND} is calculated from (a) the total dislocation line length λ necessary for forming the plastic indent and (b) the storage volume V for the GNDs, which is assumed to be proportional to the contact radius a_{c}.

$$\rho_{\text{GND}} = \frac{\lambda}{V} = \frac{(\pi h a_{\text{c}}/b)}{\frac{2}{3}\pi a_{\text{PZ}}^3} = \frac{3}{2}\frac{ha_{\text{c}}}{bf^3 a_{\text{c}}^3} = \frac{3}{2}\frac{1}{f^3}\frac{h}{a_{\text{c}}^2}. \tag{4}$$

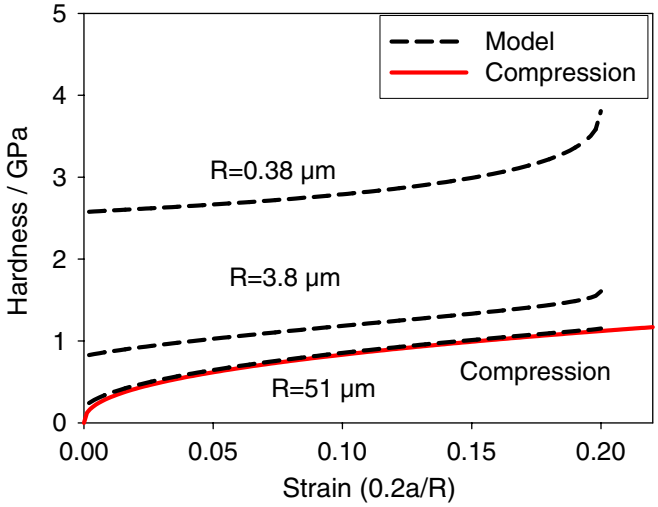

Figure 1. ISE in spherical indentation as modelled using equation (5).

The storage volume for GNDs is assumed to be half spherical, where the radius of the plastic zone is given by $a_{\text{PZ}} = fa_{\text{c}}$. The f parameter gives the average contribution of GNDs to the hardness increase at small depths, as shown later. Contrary to former discussions, the contact radius is used in conjunction with the indentation depth for describing the evolution of dislocation density with indentation depth. By doing so no additional assumptions on tip geometry are necessary and equation (4) is valid for conical as well as spherical indenters. The contact radius as used here is simply given by the indenter geometry and effects like pile-up or sink-in are not considered. For a spherical indenter geometry the contact radius is given by $a_{\text{c}} = \sqrt{2Rh - h^2}$, for conical indenters the contact radius only depends on the angle and the depth and is given by $a_{\text{c,conical}} = h\tan\beta$.

The size dependence of hardness is then calculated from the total dislocation density:

$$H_{\text{ISE}} = MC\alpha Gb\sqrt{\rho_{\text{SSD}}(\varepsilon_{\text{rep}}) + \rho_{\text{GND}}(h, f)}. \tag{5}$$

3. Modelling strength for spherical indentations

It should be noted that the deformation during spherical indentation is quite different from that of pyramidal indentation. The constraint factor depends on the strain and the size of the plastic zone is continuously changing [19]. Additionally, the strain gradients are different, continuously changing with indentation depth.

Figure 1 shows the calculated spherical indentation data from a macroscopic stress–strain curve as a function of the representative strain. In the modelling, the uniaxial stress-strain data of a coarse grained Ni poly-crystal (99.99% Ni) was used. The data for the different indenter tip radii are compared at the representative strain as given by equation (2). This way, the influence of the GNDs on the deformation behaviour can be directly compared at the same average strain in the material.

It is found that the stress increases for smaller spheres and the shape of the hardness–strain curve changes. Initially the macroscopic data and the spherical indentation data are parallel

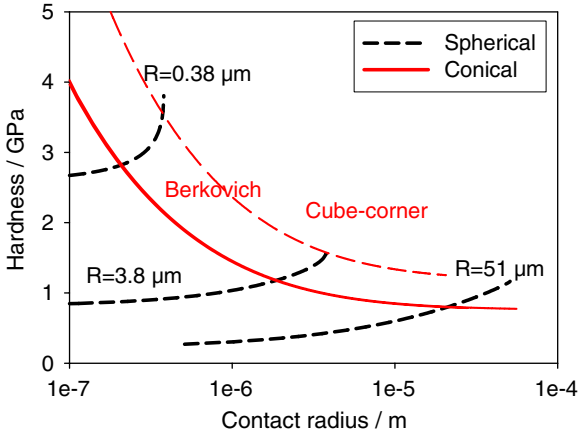

Figure 2. ISE in spherical and pyramidal indentation as modelled by equation (5).

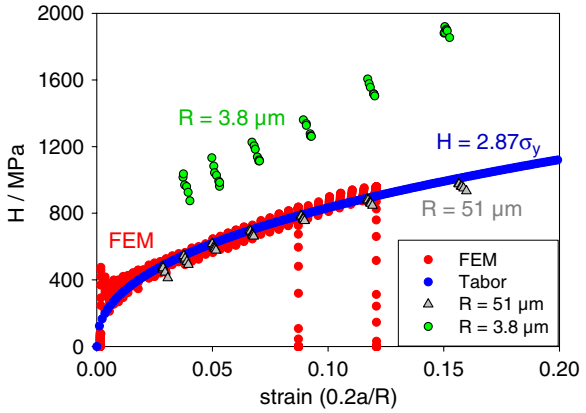

Figure 3. Comparison between simulated and experimentally determined indentation behaviour. Solid line: hardness–strain data calculated from uniaxial stress–strain behaviour (blue), red dots: finite element simulation data using macroscopic stress–strain data as input in the simulations, grey triangles: experimental data sphere radius $R = 51\,\mu$m, green dots: experimental data $R = 3.8\,\mu$m. (Colour online.)

to each other. For smaller spheres, the yield stress increases and pronounced additional work hardening is observed at higher strains. This behaviour stems from equation (5), which yields a non-linear increase in GND density with strain.

Figure 2 shows a comparison of spherical and cube-corner and Berkovich indentation as a function of contact radius. The data for Berkovich and cube-corner have been calculated using the equivalent opening angle of a conical indenter. Here the data sets for spherical and conical indenters can be compared directly without referring to the indentation depth. It is found that the spherical indentation data connects the two pyramidal curves.

4. Experimental

Indentation tests were conducted using a nanoindenter XP from MTS in load control mode. Up to five loading and unloading cycles with increasing loads were used to determine the depth dependence of hardness. Before unloading a 20 s hold segment was used to stabilize the materials response. Tip shape calibration was performed using the Hertzian contact theory for fitting the experimental load–displacement data of indentions on W up to the pop-in. W has the distinct advantage that its elastic behaviour is isotropic and the literature data on modulus can be used for calculating the reduced modulus of the diamond tungsten system. These data were compared with indentation tests on fused quartz, where the contact stiffness was used for tip shape calibration. Generally, a good agreement was found for both approaches and the larger indenters. Careful tip shape calibration has been performed on the smallest tip [20]. Here we report a similar value on the tip radius using the Hertzian approach.

A Ni poly-crystal and a W single crystal were used in this study. The materials were electrolytically polished and mounted using a crystal bond. Sphere radii of 51.7, 3.8 and 0.375 μm were used. It should be noted that the two smallest tips have a conical shape with a spherically shaped end. Due to this geometry, the tip radius is valid only up to a certain indentation depth, after which the shape is conical. The tips used thus do not allow exploiting the full range of plastic strain.

It is assumed that the annealed materials do not exhibit a great amount of pile-up and that the contact depth as determined from the indentation experiments is valid. Compression tests were performed on the well annealed Ni poly-crystal. The elastic and plastic properties were used as input parameters for finite element simulations (FEM). Details on the FE simulations can be found in [21]. This procedure was used for studying the macroscopic indentation behaviour and estimating the hardness depth relation using a continuum approach.

4.1. Macroscopic behaviour

Figure 3 summarizes the results of compression tests, finite element simulation, and indentation tests on the same material with spherical indenters with different tip radii. The solid line was calculated directly from the compression tests, using Tabor's approach with constraint $C = 2.87$. The strain for the spherical indenters was calculated using equation (2). We find that both Tabor's approach and finite element simulation yield approximately the same stress–strain curve. Moreover a good agreement is found for the simulations and the experimental results for the $R = 51\,\mu$m sphere. However, a significant size effect occurs for the $R = 3.8\,\mu$m sphere. Here the continuum approach breaks down and the material behaviour cannot be described by conventional metal plasticity.

4.2. Pop-in behaviour

Figure 4(*a*) shows experimental load–displacement data for indentations with different sphere radii. A pop-in is found for most indentations, where a higher pop-in load with a similar pop-in jump distance is found for larger sphere radii. The different slopes of the Hertzian regime in the load–displacement data also stem from the tip radii. The corresponding hardness of the material is plotted in figure 4(*b*) as a function of displacement. Here also the smaller sphere yields higher hardness values.

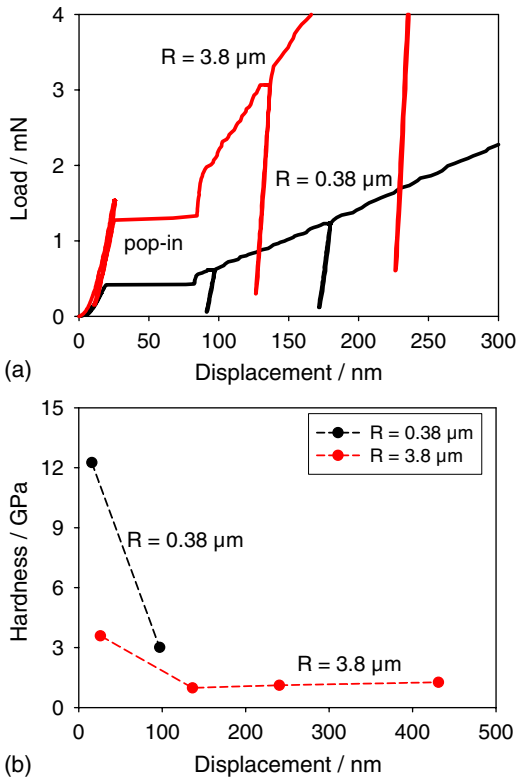

Figure 4. (*a*) Load–displacement data for two different spheres, showing a discrete transition from elastic to plastic deformation with (*b*) corresponding hardness data.

One experimental difficulty is the large pop-in occurring for the small sphere radii. The spherical part of the tip extends to a depth of only about 110 nm ($R = 0.38\,\mu$m), then the tip shape is conical. Thus in this experiments, only a small part of the tip could be used for measuring the spherical indentation response. Most of the response is purely elastic and no information on the plastic deformation resistance can be obtained for these electrolytically polished materials.

4.3. Comparison between model approach and experimental data

Figures 5 and 6 summarize the results of the spherical indentation tests with respect to our modelling approach. The macroscopic stress–strain data used were $G = 78$ GPa, $b = 0.25$ nm, $\alpha = 0.5$ and $f = 2.2$ for Berkovich and $f = 2.0$ for spherical tip shape. Generally a nice agreement is found for the experimental results and the modelling. At larger strains and smaller tip radii, higher hardness values are found for the experimental data compared with the experiments. However, the elastic–plastic transition cannot be exploited with the smaller sphere radii due to the discussed pop-in event.

Using the contact radius for comparing the different indenter geometries clearly demonstrates the general validity of the used approach. Berkovich and spherical indentation data intersect each other as would have been expected from Tabors approach.

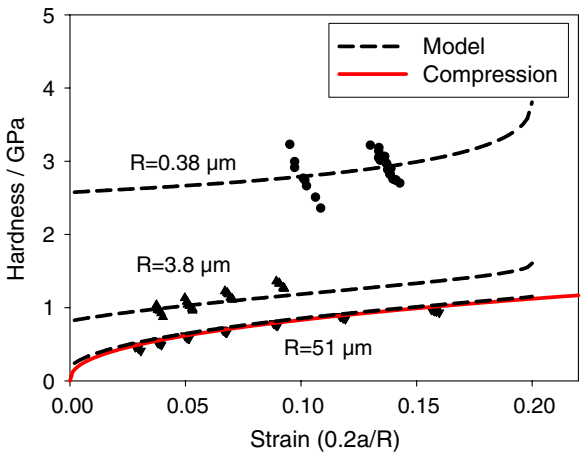

Figure 5. Hardness–strain behaviour for different sphere radii with corresponding modelled hardness–strain data.

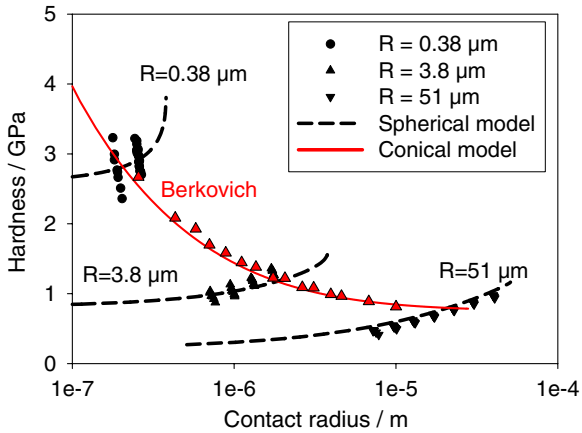

Figure 6. Hardness data as a function of contact radius for spherical and conical indentation.

5. Discussion

It is found that the combined Tabor and Taylor approach allows modelling of the size dependence of hardness for spherical and conical indentations starting from macroscopic stress–strain data. In order to describe the observed size effects, similar storage volumes for GNDs need to be considered for spherical and conical indentation, respectively. A storage volume given by $f = 2.0$ has been found to describe the experimental results from the macroscopic scale down to a tip radius of $R = 0.38\,\mu$m. Tabor's approach describes a continuous transition from elastic to elastic–plastic deformation during spherical indentation. However, at small scales a pop-in is observed, which is related to dislocation nucleation. The elastic behaviour before pop-in can be modelled in the framework of Hertzian contact theory. After pop-in, the material deforms elastic–plastically and the necessary dislocations for the formation of the plastic impression are nucleated. The hardness after pop-in and the pop-in jump width can be understood from the given theory on dislocation hardening. Depending on the local dislocation sources, a pop-in can occur well below the theoretical strength of the material. At the pop-in, the elastically energy is released and stored in the created dislocation structure.

For large spheres, the classical work hardening is found after the pop-in event. For small spheres, a pop-in jump width of 100 nm already leads to large a/R values. Furthermore, an overshot in displacement is found right after the pop-in [22]. Depending on how 'close' unloading is performed after the pop-in, a different hardness value can be measured. Part of the relatively large scatter of hardness data for the 0.38 μm spherical indenter at small indentation depths might be related to this.

6. Conclusions

In this paper size effects observed during indentation testing have been discussed for spherical indentation in comparison with conical indentation. In the modelling approach the hardness is modelled for both indenter geometries starting from the macroscopic uniaxial stress–strain data using Taylor dislocation hardening in conjunction with Tabor's concept on representative strain. The depth dependence of hardness is then introduced via Ashby's concept on GNDs in a corrected Nix/Gao approach, where the storage volume for GNDs is considered.

It is found that for a tip radius of 51 μm the tested Ni poly-crystal exhibits a macroscopic behaviour and the indentation response can be modelled from macroscopic stress–strain data via Tabor's approach or finite element simulations. At smaller sphere radii, the continuum approach breaks down and higher hardness levels are found for smaller sphere radii. Moreover, a pop-in behaviour is observed in the load–displacement data, which indicates the transition from elastic to plastic deformation due to the nucleation of dislocations. The continuum concept of Tabor on the elastic–plastic transition for spherical indentation is no longer valid. The initial deformation, however, is still purely elastic, since the deformed material has a low dislocation density. For plastic deformation, dislocations have to be nucleated, which happens in a displacement burst—the so-called pop-in behaviour. The hardness after the pop-in can be modelled assuming a relatively small storage volume for GNDs for spherical indentation. A storage volume given by $f = 2.0$ describes the experimental observed size effect best. Using the contact radius, spherical and conical indentations are directly comparable and similar stress levels are found for the same contact radius.

Acknowledgments

This work has been sponsored by DFG under contract Du 424/3-1 and SHaRe proposal 06Durst. The authors are grateful for the helpful assistance and discussion with B Backes, S Shim, J Strader, H Bin and E Herbert.

References

[1] Fleck N A, Muller G M, Ashby M F and Hutchinson J W 1994 Strain gradient plasticity: theory and experiment *Acta Metall. Mater.* **42** 475–87

[2] Gane N and Bowden F P 1968 Microdeformation of solids *J. Appl. Phys.* **39** 1432–5

[3] Page T F, Oliver W C and McHargue C J 1992 Deformation behaviour of ceramic crystals subjected to very low load (nano)indentations *J. Mater. Res.* **7** 450–73

[4] Stelmashenko N A, Walls M G, Brown L M and Milman Y V 1993 Microindentations on W and mo oriented single crystals: an STM study *Acta Metall. Mater.* **41** 2855–65

[5] Nix W D and Gao H 1998 Indentation size effects in crystalline materials: a law for strain gradient plasticity *J. Mech. Phys. Solids* **46** 411–25

[6] Ashby M F 1970 Deformation of plastically no-homogeneous materials *Phil. Mag.* **21** 399–424

[7] Durst K, Backes B and Göken M 2005 Indentation size effect in metallic materials: correcting for the size of the plastic zone *Scr. Mater.* **52** 1093–109

[8] Durst K, Backes B, Franke O and Göken M 2006 Indentation size effect in metallic materials: modeling strength from pop-in to macroscopic hardness using geometrically necessary dislocations *Acta Mater.* **54** 2547–55

[9] Lim Y Y, Bushby A J and Chaudhri M M 1998 *Mater. Res. Soc. Symp. Proc.* **522** 145–50

[10] Lim Y Y and Chaudhri M M 1999 The effect of the indenter load on the nanohardness of ductile metals: an experimental study on polycrystalline work-hardened and annealed oxygen-free copper *Phil. Mag.* A **79** 2979–3000

[11] Yang B and Vehoff H 2007 Dependence of nanohardness upon indentation size and grain size—a local examination of the interaction between dislocations and grain boundaries *Acta Mater.* **55** 849–56

[12] Liu Y and Ngan A H W 2001 Depth dependence of hardness in copper single crystals measured by nanoindentation *Scr. Mater.* **44** 237–41

[13] Spary I J, Bushby A J and Jennett N M 2006 On the indentation size effect in spherical indentation *Phil. Mag.* A **86** 5581–93

[14] Zaafarani N, Raabe D, Singh R N, Roters F and Zaefferer S 2006 Three-dimensional investigation of the texture and microstructure below a nanoindent in a cu single crystal using 3D EBSD and crystal plasticity finite element simulations *Acta Mater.* **54** 1863–76

[15] Kiener D, Pippan R, Motz C and Kreuzer H 2006 Microstructural evolution of the deformed volume beneath microindents in tungsten and copper *Acta Mater.* **54** 2801–11

[16] Swadener J G, George E P and Pharr G M 2002 The correlation of the indentation size effect measured with indenters of various shapes *J. Mech. Phys. Solids* **50** 681–94

[17] Atkins A G and Tabor D 1965 Plastic indentation in metals with cones *J. Mech. Phys. Solids* **13** 149–64

[18] Mughrabi H 2004 On the current understanding of strain gradient plasticity *Mater. Sci. Eng.* A **387–389** 209–13

[19] Durst K, Göken M and Pharr G M 2002 Finite element simulation of spherical indentation in the elastic-plastic transition *Z. Metallk./Mater. Res. Adv. Tech.* **93** 857–61

[20] Herbert E G, Oliver W C and Pharr G M 2006 On the measurement of yield strength by spherical indentation *Phil. Mag.* **86** 5521–39

[21] Backes B, Durst K and Göken M 2006 Determination of plastic properties of polycrystalline metallic materials by nanoindentation: experiments and finite element simulations *Phil. Mag.* **86** 5541–51

[22] Bahr D F, Kramer D E and Gerberich W W 1998 Non-linear deformation mechanisms during nanoindentation *Acta Mater.* **46** 3605–17